


Resistivity, Seebeck coefficient, and thermal conductivity of platinum at high pressure and temperature

Hitoshi Gomi (五味齋) * and Takashi Yoshino (芳野極)

Institute for Planetary Materials, Okayama University, Misasa, Tottori 682-0193, Japan



(Received 26 January 2019; revised manuscript received 17 October 2019; published 5 December 2019)

Platinum (Pt) is one of the most widely used functional materials for high-pressure and high-temperature experiments. Despite the crucial importance of its transport properties, both experimental and theoretical studies are very limited. In this study, we conducted density functional theory calculations on the electrical resistivity, the Seebeck coefficient, and the thermal conductivity of solid face-centered cubic Pt at pressures up to 200 GPa and temperatures up to 4800 K by using the Kubo-Greenwood formula. The thermal lattice displacements were treated within the alloy analogy, which is represented by means of the Korringa-Kohn-Rostoker method with the coherent potential approximation. The electrical resistivity decreases with pressure and increases with temperature. These two conflicting effects yield a constant resistivity of $\sim 70 \mu\Omega \text{ cm}$ along the melting curve. Both pressure and temperature effects enhance the thermal conductivity at low temperatures, but the temperature effect becomes weaker at high temperatures. Although the pressure dependence of the Seebeck coefficient is negligibly small at temperatures below $\sim 1500 \text{ K}$, it becomes larger at higher temperatures. It requires a calibration of a thermocouple such as Pt-Rh in high-pressure and -temperature experiments.

DOI: [10.1103/PhysRevB.100.214302](https://doi.org/10.1103/PhysRevB.100.214302)

I. INTRODUCTION

Platinum is one of the most important functional materials in high-pressure geoscience and solid state physics, because of its chemical and structural stability with respect to pressure and temperature. The application includes, for example, pressure markers [1–3], laser absorbers [4], electrodes [5], capsules for hydrous systems [6], and thermocouples [7] in high-pressure apparatuses.

Its transport properties are important and closely related with each other [8,9] and, thus, extensive studies are reported for Pt at ambient pressure [10–23]. For example, the electrical resistivity, the Seebeck coefficient, and the thermal conductivity are reported to be $10.87 \mu\Omega \text{ cm}$, $-5.28 \mu\text{V/K}$, and $71.6 \text{ W m}^{-1} \text{ K}^{-1}$ at 300 K, respectively [10–12]. However, high-pressure measurements on the electrical resistivity [24], the Seebeck coefficient [7], and the thermal conductivity [25] are very limited. Furthermore, recent high-pressure and -temperature measurements of the electrical resistivity [26] and the thermal conductivity [27] of Fe were inconsistent with each other, because of the technical difficulties for measurements of these transport properties [28].

From the point of view of first-principles calculations, the resistivity and the thermal conductivity of solid Fe at high pressure and temperature have been computed either by means of the density functional perturbation theory (DFPT) [5,29] or the first-principles molecular dynamics (FPMD) combined with the Kubo-Greenwood formula [30]. The recently proposed alloy analogy method allows us to simulate the phonon scattering within the coherent potential approximation (CPA) [31–33]. This method was applied to Fe at high pressure and

temperature to determine the electrical and thermal transport properties of the Earth's core [34,35]. It is worth mentioning that the alloy analogy method is suitable to calculate the Seebeck coefficient. Until recently, most of the first-principles studies of the Seebeck coefficient have been based on the Boltzmann equation with the assumption that the mean free time of electrons is constant with respect to the energy [36,37]. This is because of the technical difficulty to calculate the electron scattering. Wang *et al.* [37] demonstrated that the Seebeck coefficient is a thermodynamic quantity that can be computed solely on the electron density of states (DOS). However, the electron DOS depends on the scattering. Kou and Akai [33] successfully calculated the Seebeck coefficients of transition metals with electron scattering by using the alloy analogy method at ambient pressure.

As shown above, the previous studies on the electronic transport properties (electrical resistivity, Seebeck coefficient, and thermal conductivity) of Pt are limited at high pressure. Therefore, we calculated the electronic transport properties up to 200 GPa and 4800 K by means of the Korringa-Kohn-Rostoker (KKR) method combined with the alloy analogy within the coherent potential approximation (CPA) [32,33]. Up to 100 GPa, the transport properties are calculated with a 10-GPa step in order to supply reference data set for a Kawai-type multi-anvil apparatus (KMA) experiments. As an example, we discuss the problem of the temperature determination by using a Pt-Rh thermocouple under the deep lower mantle pressure and temperature conditions. We further calculated the transport properties at 150 and 200 GPa, which is sufficient for diamond-anvil cell (DAC) experiments.

II. METHODS

Within the alloy analogy model [32,33], the thermal atomic displacements were represented as a discrete set of

*hitoshi.gomi@okayama-u.ac.jp

N_v displacement vectors $\Delta \mathbf{R}_v(T)$. The band structure of Pt with finite temperature lattice vibrations can be, thus, represented as a pseudoalloy with the N_v pseudocomponents with $|\Delta \mathbf{R}_v(T)| = \sqrt{\langle u^2 \rangle}$ by the coherent potential approximation (CPA). Using the Debye theory, the mean square displacement was represented as

$$\langle u^2 \rangle = \frac{9\hbar^2}{mk_B\Theta_D} \left\{ \left(\frac{T}{\Theta_D} \right) \int_0^{\Theta_D/T} \frac{z}{\exp(z) - 1} dz + \frac{1}{4} \right\}, \quad (1)$$

where \hbar is the reduced Planck's constant (the Dirac's constant), m is the atomic mass, k_B is the Boltzmann's constant, Θ_D is the Debye temperature, and T is temperature. Neglecting the zero-point vibration, it becomes

$$\langle u^2 \rangle = \frac{9\hbar^2 T}{mk_B\Theta_D^2}. \quad (2)$$

Following the previous calculations [32,33], we set $N_v = 14$ for most of the present calculations. We also tested $N_v = 4, 6, 8, 12,$ and 20 , for convergence at 0 GPa, whose coordinates are identical to the vertex positions of regular polyhedrons that are inscribed in a sphere with the radius of $r = \sqrt{\langle u^2 \rangle}$. The lattice parameter and the Debye temperature are obtained from the experimentally determined equation of state of Pt at each

pressure and temperature condition [2]. The Kohn-Sham equation was solved by means of the Korringa-Kohn-Rostoker (KKR) Green function method, which is implemented in the AKAIKKR package [38]. The Perdew-Burke-Ernzerhof (PBE) type of generalized gradient approximation (GGA) was adapted to the exchange-correlation potential [39]. The crystal potential was approximated by using the atomic spherical approximation (ASA). The maximum angular momentum quantum number was set to $l = 3$. Relativistic effects were considered in the scalar relativistic approximation. The conductivity was calculated from the Kubo-Greenwood formula with the vertex correction [33,36,40–42]. By using K_n , the electrical resistivity ρ , the Seebeck coefficient S , and the thermal conductivity k can be calculated as follows,

$$\frac{1}{\rho} = K_0, \quad (3)$$

$$S = -\frac{1}{eT} \frac{K_1}{K_0}, \quad (4)$$

$$k = \frac{1}{e^2 T} \left(K_2 - \frac{K_1^2}{K_0} \right), \quad (5)$$

$$K_n = \int_{-\infty}^{\infty} \sigma(\varepsilon) (\varepsilon - \mu)^n \left(-\frac{\partial f}{\partial \varepsilon} \right) d\varepsilon, \quad (6)$$

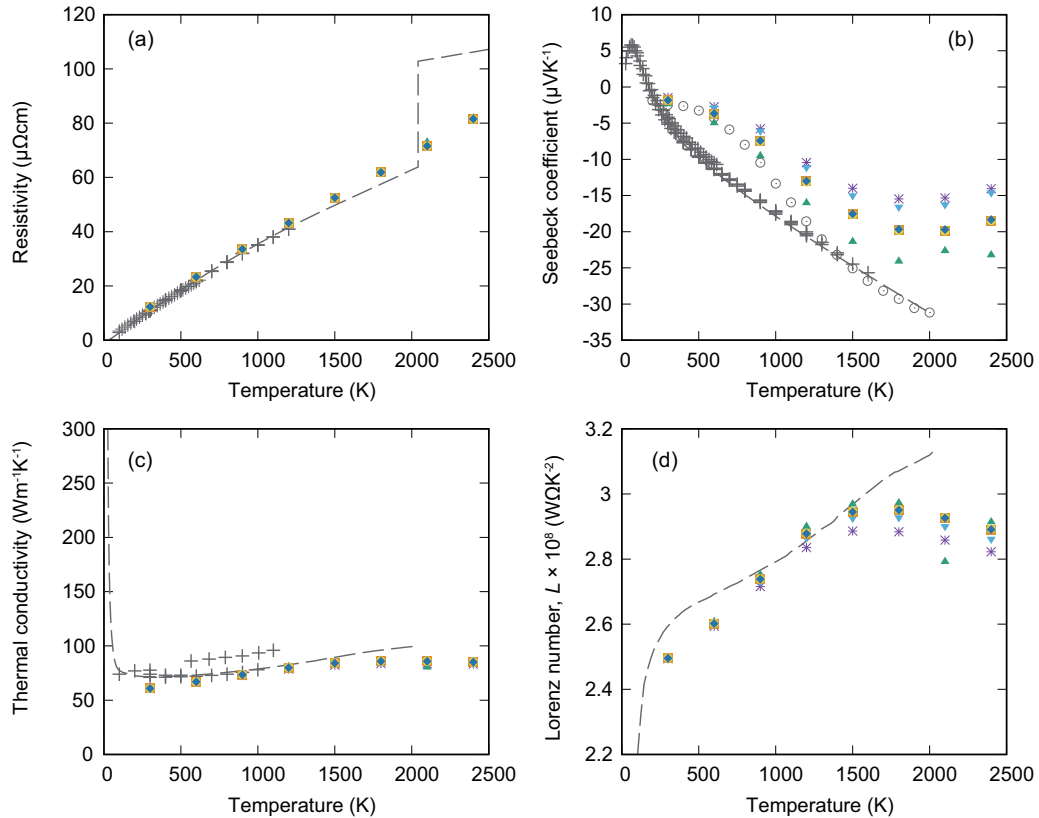


FIG. 1. (a) Electrical resistivity, (b) Seebeck coefficient, (c) thermal conductivity, and (d) Lorenz number of Pt as function of temperature at 0 GPa. Colored symbols are present calculations with $N_v = 4$ (*), 6 (▲), 8 (▼), 12 (■), 14 (•), and 20 (◆). These symbols are largely overlapped in (a), (c), whereas they are somewhat scattered in (b), (d). Gray broken lines indicate the literature data of the electrical resistivity [10], the Seebeck coefficient [11], the thermal conductivity [12], and the Lorenz number [10,12]. Cross symbols are previous experiments of resistivity [13,14,16–19], Seebeck coefficient [15–17,20,21], and thermal conductivity measurements [14,18,22,23]. Open gray circles indicate the previous calculation [33]. Note that the results are almost independent of the N_v except for the Seebeck coefficient, and consistent with the literature.

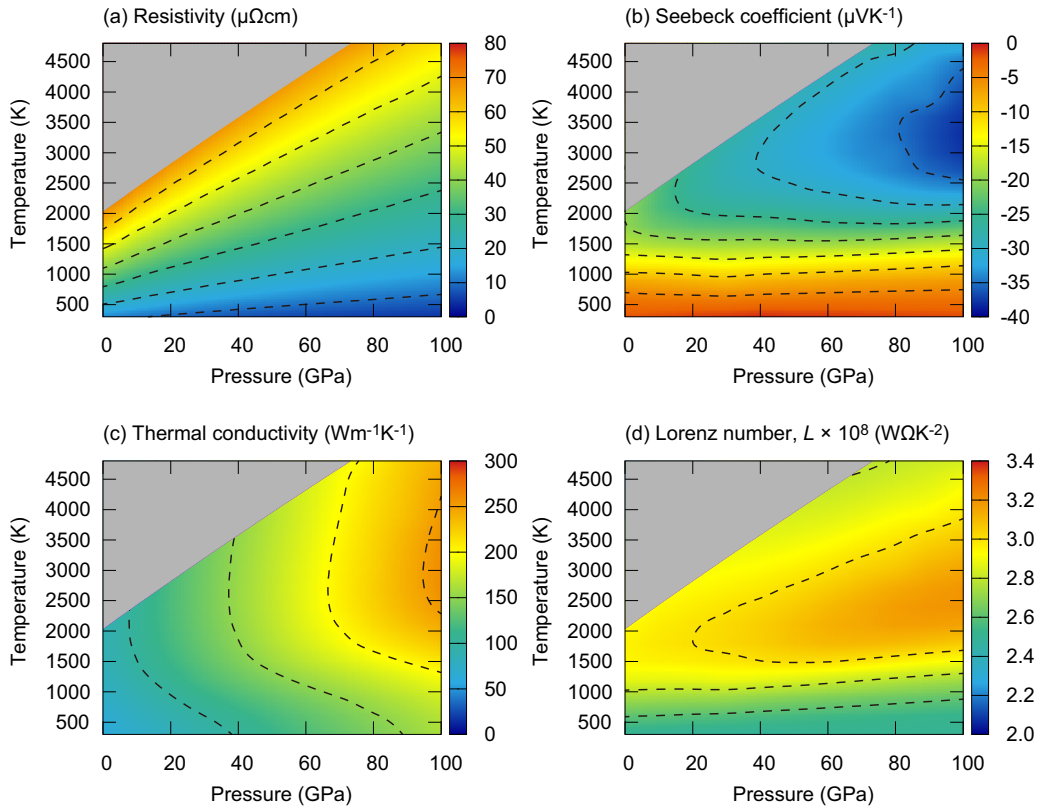


FIG. 2. Pressure and temperature dependence of (a) the electrical resistivity, (b) the Seebeck coefficient, (c) the thermal conductivity, and (d) the Lorenz number of solid fcc Pt up to 100 GPa. The gray region represents the liquid stability field [43]. All the source data are in Tables I–IV.

where $\sigma(\varepsilon)$ is the conductivity, ε is the energy, μ is the chemical potential, and f is the Fermi-Dirac distribution function. For the conductivity calculation, 65 701 k points were used in the irreducible Brillouin zone. The energy-dependent conductivity $\sigma(\varepsilon)$ is calculated within the complex energy mesh with 201 energy points. The real part of the energy range is from $\varepsilon_F - 10\varepsilon_{\text{HWHM}}$ to $\varepsilon_F + 10\varepsilon_{\text{HWHM}}$, where ε_F is the Fermi energy and $\varepsilon_{\text{HWHM}} = \ln(3 + 2^{3/2})k_B T$ is the half width at half maximum (HWHM) of $\partial f/\partial \varepsilon$. A small imaginary part, i.e., $\eta = 0.000\,01$ Ry, was attached to the energy mesh.

III. RESULTS AND DISCUSSIONS

The results of the present calculations with $N_v \geq 12$ well reproduce the literature data at ambient pressure [10–12]. Figure 1 shows the results of the electrical resistivity, the Seebeck coefficient, the thermal conductivity, and the Lorenz number of Pt at 0 GPa with various N_v compared with literature values [10–12]. The electrical resistivity increases with increasing temperature, and shows excellent agreement with previous experiments [10] up to a melting temperature of $T = 2042$ K [43,44] [Fig. 1(a)]. It is worth mentioning that $N_v = 4$ is enough for the electrical resistivity calculation. The calculated Seebeck coefficients are always negative, and their absolute values increase with increasing temperature. Our calculations reproduce the general trends of temperature dependence, but are systematically higher than the value determined from experiments [11]. This systematic error may relate to the effect of thermal expansion [37]. Wang *et al.* [37]

suggested that the isobaric Seebeck coefficient contains the constant volume contribution and thermal expansion contribution, which is 10% – 20% of the former. In this study, we calculated the constant volume contribution only. In contrast to the electrical resistivity, the Seebeck coefficient depends on N_v , and $N_v \geq 12$ is required for the convergence. The calculated thermal conductivity is insensitive to temperature, which is consistent with the literature value [12] [Fig. 1(c)]. The calculated thermal conductivity is also insensitive to N_v . Because we calculated the electrical resistivity and the thermal conductivity separately, it is possible to evaluate the pressure and temperature dependences of the Lorenz number, $L(P, T) = \rho(P, T)k(P, T)/T$. The Lorenz number is calculated to be $L = 2.50 \times 10^{-8} \text{ W } \Omega \text{ K}^{-2}$ at 0 GPa and 300 K, which is very close to the Sommerfeld value of the Lorenz number $L_{\text{Sommerfeld}} = \pi^2 k_B^2 / 3e^2 \cong 2.445 \times 10^{-8} \text{ W } \Omega \text{ K}^{-2}$, where e is an elementary charge. The Lorenz number increases with increasing temperature, which indeed exhibits temperature dependence. This behavior is consistent with the Lorenz number calculated from the literature data [10,12] [Fig. 1(d)].

Considering the convergence with respect to N_v at 0 GPa, we adopted $N_v = 14$ for calculations at high pressure and high temperature up to the melting temperature [43]. The results up to 100 GPa are shown in Fig. 2, and higher-pressure values are plotted in Fig. 3. All the numerical values of the present calculation with $N_v = 14$ are found in Tables I–IV.

Figure 4 shows the pressure dependence of the electrical resistivity at 300 K. The electrical resistivity decreases with increasing pressure, which is consistent with a previous

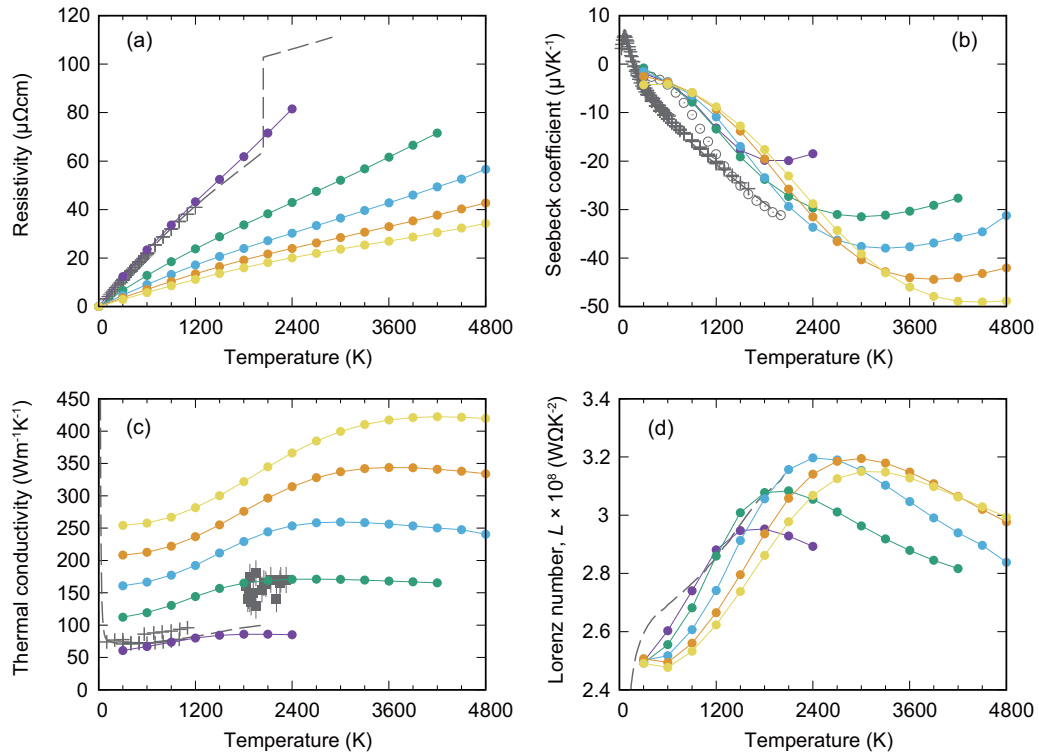


FIG. 3. Pressure and temperature dependence of (a) the electrical resistivity, (b) the Seebeck coefficient, (c) the thermal conductivity, and (d) the Lorenz number of solid fcc Pt up to 200 GPa. Pressure conditions are 0 (purple), 50 (green), 100 (cyan), 150 (orange), and 200 GPa (yellow). Previous studies at ambient pressure are also plotted for comparison. Gray broken lines indicate the literature data of the electrical resistivity [10], the Seebeck coefficient [11], the thermal conductivity [12], and the Lorenz number [10,12]. Cross symbols are previous experiments of resistivity [13,14,16–19], Seebeck coefficient [15–17,20,21], and thermal conductivity measurements [14,18,22,23]. Open gray circles indicate the previous calculation [33]. Gray squares represent the previous thermal conductivity measurements at high pressures between 35 and 55 GPa [25].

measurement result [24]. Considering both pressure and temperature effects, the electrical resistivity increases with increasing temperature, whereas it decreases with increasing

pressure [Fig. 2(a)]. At high temperatures, isoresistivity curves become parallel to the melting curve determined by Belonoshko and Rosengren [43], which is consistent with

TABLE I. Electrical resistivity of fcc Pt at high pressure and temperature ($\mu\Omega\text{ cm}$).

T (K)	P (GPa)												
	0	10	20	30	40	50	60	70	80	90	100	150	200
300	12.31	10.45	9.11	8.10	7.30	6.66	6.13	5.68	5.29	4.96	4.66	3.61	2.94
600	23.34	19.88	17.40	15.49	14.01	12.83	11.83	10.98	10.25	9.62	9.06	7.04	5.76
900	33.57	28.55	24.94	22.19	20.15	18.50	17.11	15.92	14.90	14.01	13.23	10.37	8.53
1200	43.18	36.72	32.05	28.53	25.91	23.78	21.99	20.49	19.20	18.08	17.10	13.51	11.18
1500	52.48	44.51	38.85	34.65	31.43	28.79	26.59	24.75	23.18	21.84	20.65	16.45	13.68
1800	61.84	52.13	45.44	40.51	36.73	33.63	31.01	28.82	26.94	25.36	23.99	19.15	16.00
2100	71.55	59.91	51.99	46.25	41.88	38.33	35.33	32.80	30.61	28.75	27.15	21.65	18.15
2400	81.51	67.86	58.59	51.96	46.94	42.92	39.55	36.68	34.22	32.08	30.24	24.00	20.11
2700		76.03	65.37	57.75	52.02	47.49	43.74	40.55	37.83	35.42	33.34	26.23	21.94
3000			72.32	63.67	57.20	52.11	47.93	44.41	41.49	38.77	36.46	28.44	23.66
3300				69.73	62.47	56.81	52.19	48.31	45.03	42.15	39.61	30.67	25.33
3600					68.02	61.62	56.52	52.26	48.64	45.55	42.79	32.96	27.00
3900					73.42	66.53	60.96	56.29	52.35	49.21	46.04	35.32	28.70
4200						71.53	65.46	60.40	56.12	52.58	49.36	37.74	30.46
4500							70.05	64.62	59.96	56.02	52.65	40.22	32.35
4800								69.79	65.13	59.63	56.63	42.75	34.25

TABLE II. Seebeck coefficient of fcc Pt at high pressure and temperature ($\mu\text{V K}^{-1}$).

T (K)	P (GPa)												
	0	10	20	30	40	50	60	70	80	90	100	150	200
300	-1.87	-1.49	-1.12	-0.89	-0.51	-0.77	-0.88	-1.05	-1.23	-1.39	-1.54	-2.50	-4.27
600	-3.77	-4.12	-4.21	-4.36	-4.08	-3.93	-3.82	-3.74	-3.67	-3.63	-3.60	-3.73	-4.13
900	-7.55	-7.93	-8.46	-8.96	-8.23	-7.84	-7.52	-7.21	-6.93	-6.68	-6.47	-5.90	-5.88
1200	-13.19	-13.31	-13.81	-14.26	-13.72	-13.39	-12.97	-12.45	-11.90	-11.37	-10.89	-9.30	-8.81
1500	-17.74	-18.59	-18.98	-19.09	-18.97	-19.15	-19.15	-18.82	-18.25	-17.56	-16.97	-13.83	-12.74
1800	-19.88	-22.17	-23.07	-23.33	-23.38	-23.80	-24.30	-24.47	-24.51	-24.09	-23.43	-19.56	-17.59
2100	-19.89	-23.68	-25.57	-26.43	-26.77	-27.28	-28.00	-28.56	-29.29	-29.51	-29.35	-25.81	-23.10
2400	-18.50	-23.56	-26.60	-28.17	-28.96	-29.67	-30.48	-31.38	-32.38	-33.17	-33.65	-31.54	-28.82
2700		-22.37	-26.33	-28.69	-30.02	-31.01	-31.97	-32.99	-34.11	-35.29	-36.29	-36.61	-34.29
3000			-25.22	-28.27	-30.12	-31.46	-32.61	-33.72	-34.27	-36.28	-37.61	-40.38	-39.13
3300				-27.18	-29.53	-31.17	-32.55	-33.78	-34.82	-36.43	-37.98	-42.80	-43.05
3600					-28.14	-30.34	-31.94	-33.33	-34.61	-36.13	-37.67	-44.06	-45.97
3900					-26.87	-29.11	-30.86	-32.46	-33.85	-34.19	-36.87	-44.40	-47.90
4200						-27.62	-29.59	-31.28	-32.77	-33.72	-35.71	-44.05	-48.93
4500							-28.07	-29.81	-31.47	-32.86	-34.57	-43.21	-49.09
4800								-26.98	-28.13	-31.50	-31.22	-42.02	-48.83

the recent laser-heated diamond-anvil cell measurement and theoretical calculations [44–46]. This gives a constant resistivity value of $\sim 70 \mu\Omega \text{ cm}$ along the melting curve. This phenomenon is consistent with the model suggested by Stacey and Anderson [47], which predicts that the electrical resistivity of Fe becomes constant along the melting curve. McWilliams *et al.* [25] applied the Stacey's constant resistivity model [47] to Pt. This idea is initially proposed by Stacey and Anderson [47] based on the Lindeman's melting criterion, which suggests that melting occurs when the mean square displacement of ions reaches a specific value. Because the electrical resistivity also depends on the mean square displacement, Stacey and Anderson [47] considered that the phonon-contributed resistivity of pure metals becomes constant along the melting curve. However, the model cannot be

used for metals that exhibit strong resistivity saturation behavior such as Fe [5]. The resistivity saturation phenomenon is predicted to occur at high resistivity comparable with the Ioffe-Regel condition ($\sim 150 \mu\Omega \text{ cm}$) [48]. The resistivity of Pt at the melting temperature is $\sim 70 \mu\Omega \text{ cm}$ at ambient pressure. This value is sufficiently smaller than $\sim 150 \mu\Omega \text{ cm}$. Indeed, the temperature dependence of ambient pressure resistivity is almost free from the saturation behavior. Our calculation predicted that the resistivity of Pt is constant along the melting curve; therefore, we considered that the effect of saturation is small within the pressure and temperature conditions calculated in this study. Therefore, the Stacey's constant resistivity model [47] is applicable for Pt.

Figure 5 represents the temperature dependence of the thermal conductivity at 0, 50, and 100 GPa. The thermal

TABLE III. Thermal conductivity of fcc Pt at high pressure and temperature ($\text{W m}^{-1} \text{K}^{-1}$).

T (K)	P (GPa)												
	0	10	20	30	40	50	60	70	80	90	100	150	200
300	60.83	71.40	81.78	92.06	101.90	112.31	122.21	132.01	141.71	151.33	160.91	208.20	254.32
600	66.92	78.33	89.12	99.80	109.83	119.51	129.14	138.67	148.10	157.45	166.70	212.41	257.89
900	73.47	86.15	98.50	110.57	120.65	130.46	140.12	149.63	158.99	168.21	177.34	222.18	267.09
1200	80.05	93.89	107.75	121.47	133.23	144.31	154.69	164.52	174.00	183.23	192.37	236.74	281.53
1500	84.25	99.74	114.56	129.14	143.11	156.77	169.46	180.94	191.47	201.31	211.64	254.90	300.16
1800	85.94	103.02	118.84	134.20	149.33	164.74	179.89	193.81	206.90	218.58	229.27	275.91	321.91
2100	85.94	104.11	120.92	137.01	152.75	168.95	185.51	201.23	217.06	231.21	244.16	296.68	344.62
2400	85.19	104.00	121.61	138.21	154.34	170.83	187.94	205.19	222.26	238.48	253.67	314.04	366.09
2700		103.25	121.27	138.27	154.63	171.20	188.39	206.19	224.00	241.47	258.35	327.87	384.64
3000			120.46	137.66	154.11	170.63	187.71	205.51	222.10	241.67	259.52	337.05	399.39
3300				136.72	153.19	169.51	186.38	203.97	221.39	240.18	258.53	342.09	410.10
3600					151.70	168.20	184.75	202.00	219.79	238.12	256.28	343.85	417.10
3900					150.80	166.77	182.90	199.88	217.46	233.08	253.40	343.23	420.96
4200						165.38	181.27	197.76	214.98	231.25	250.15	341.06	422.27
4500							179.64	195.67	212.54	229.53	247.54	337.89	421.34
4800								191.49	206.62	227.08	240.61	334.22	419.48

TABLE IV. Lorenz number of fcc Pt at high pressure and temperature, $L \times 10^8$ ($\text{W } \Omega \text{ K}^{-2}$).

T (K)	P (GPa)												
	0	10	20	30	40	50	60	70	80	90	100	150	200
300	2.50	2.49	2.48	2.48	2.48	2.49	2.50	2.50	2.50	2.50	2.50	2.51	2.49
600	2.60	2.60	2.58	2.58	2.56	2.56	2.55	2.54	2.53	2.52	2.52	2.49	2.48
900	2.74	2.73	2.73	2.73	2.70	2.68	2.66	2.65	2.63	2.62	2.61	2.56	2.53
1200	2.88	2.87	2.88	2.89	2.88	2.86	2.84	2.81	2.78	2.76	2.74	2.67	2.62
1500	2.95	2.96	2.97	2.98	3.00	3.01	3.00	2.98	2.96	2.93	2.91	2.80	2.74
1800	2.95	2.98	3.00	3.02	3.05	3.08	3.10	3.10	3.10	3.08	3.06	2.94	2.86
2100	2.93	2.97	2.99	3.02	3.05	3.08	3.12	3.14	3.16	3.17	3.16	3.06	2.98
2400	2.89	2.94	2.97	2.99	3.02	3.05	3.10	3.14	3.17	3.19	3.20	3.14	3.07
2700		2.91	2.94	2.96	2.98	3.01	3.05	3.10	3.14	3.17	3.19	3.19	3.13
3000			2.90	2.92	2.94	2.96	3.00	3.04	3.07	3.12	3.15	3.19	3.15
3300				2.89	2.90	2.92	2.95	2.99	3.02	3.07	3.10	3.18	3.15
3600					2.87	2.88	2.90	2.93	2.97	3.01	3.05	3.15	3.13
3900					2.84	2.84	2.86	2.89	2.92	2.94	2.99	3.11	3.10
4200						2.82	2.83	2.84	2.87	2.89	2.94	3.06	3.06
4500							2.80	2.81	2.83	2.86	2.90	3.02	3.03
4800									2.78	2.80	2.82	2.84	2.99

conductivity is strongly enhanced by applying pressure, whereas the temperature effect is insignificant. The previous measurements of the thermal conductivity at 35, 50, and 55 GPa are also plotted for comparison [25]. Our calculation is consistent with the previous measurement result. Figure 2(c) shows the pressure and temperature dependence of the thermal conductivity. The thermal conductivity increases with increasing pressure and temperature at low temperatures. McWilliams *et al.* [25] fit their thermal conductivity data to the simple planar function: $k = aP + bT + c$. However, our calculation predicts that such a simple expression cannot apply at high temperature, because its thermal conductivity is almost insensitive to the temperature at high temperature. This can be understood as follows: the Bloch-Grüneisen law predicts linear temperature dependence of the electrical resistivity at high temperatures, which is cancelled out with the linear temperature dependence of the Wiedemann-Franz law. The calculated Lorenz number as functions of pressure and temperature is

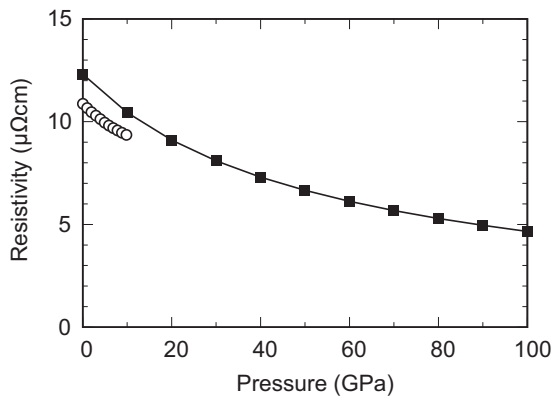


FIG. 4. Electrical resistivity of Pt as function of pressure at 300 K. Solid line with filled square symbols represents the present calculation and open circles indicate the previous measurements [24].

shown in Fig. 2(d). Similar to the ambient pressure, the Lorenz number exhibits temperature dependence. It increases with temperature, and reaches a maximum value around 1500 K. Then, it is flattening, and finally its value gets smaller at higher temperature. Such temperature-dependent Lorenz number is already reported at high pressure [42,49]. Within the calculated pressure and temperature range, the maximum value was obtained to be $L = 3.20 \times 10^{-8} \text{ W } \Omega \text{ K}^{-2}$ at 100 GPa and 2400 K, which is 30% higher than the Sommerfeld value of $L_{\text{Sommerfeld}} \cong 2.445 \times 10^{-8} \text{ W } \Omega \text{ K}^{-2}$.

Figure 2(b) shows the Seebeck coefficient as functions of pressure and temperature. At low temperatures ($T \leq 1500$ K), the Seebeck coefficient is almost pressure independent. However, it shows strong pressure dependence at temperature higher than 1500 K. Pt is widely used as a R -type

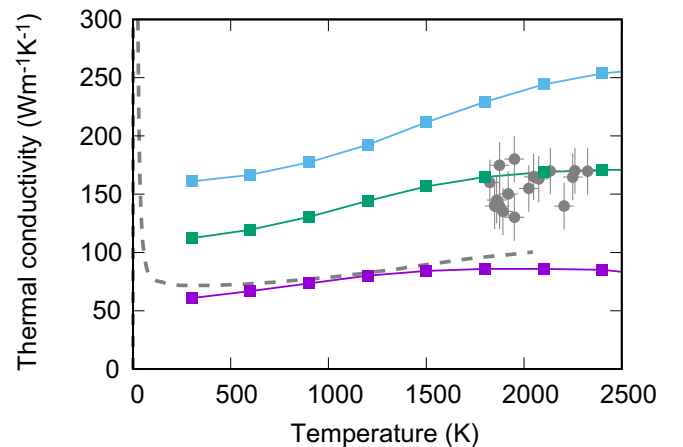


FIG. 5. Thermal conductivity of Pt at high pressure as a function of temperature. Square symbols are present calculations at 0 (purple), 50 (green), and 100 GPa (cyan). Gray broken line indicates the literature data at ambient pressure [12]. Gray circles represent the previous measurements at high pressures between 35 and 55 GPa [25].

(Pt-Pt87Rh13) or *S*-type (Pt-Pt90Rh10) thermocouple in a high-pressure and high-temperature experimental apparatus such as a piston cylinder or a Kawai-type multianvil apparatus (KMA). However, no pressure correction has been made, so far [50]. A single wire method has been conducted to measure the electromotive force (EMF) at high pressure, but because of its technical difficulty, the maximum pressure condition is restricted to be 7.2 GPa [51] and the temperature range is less than 1273 K [7,50,51]. Also, intercomparison of multiple thermocouples has been carried out only up to 15 GPa and 2073 K [52]. On the other hand, recent technical advances of KMA have expanded the range of experimental pressure and temperature. By using sintered diamond cubic anvils, the maximum pressure reaches more than 120 GPa [53]. For high-temperature generation, a boron-doped diamond heater enables us to heat the sample to ~ 4000 K [54]. Indeed, such a high-pressure and high-temperature condition corresponds to the region where the Seebeck coefficient exhibits strong pressure dependence. Let us estimate the significance of the pressure dependence of the Seebeck coefficient on the temperature reading by using the Pt-Rh thermocouple. The Seebeck coefficient of Pt is $-31.12 \mu\text{V K}^{-1}$ at 40 GPa and 3000 K. With a compression to 100 GPa at the identical temperature, it becomes $-37.61 \mu\text{V K}^{-1}$, which is $\sim 20\%$ enhancement. Assuming that the Seebeck coefficient of the Pt-Rh alloy exhibits the same pressure dependence, a $\sim 20\%$ enhancement on the relative Seebeck coefficient results in a ~ 600 K enhancement on the apparent temperature. This uncertainty is larger than the typical temperature error (~ 200 K) in laser-heated diamond-anvil cell experiments [4]. Therefore, developments of temperature measurement become one of the most important tasks for high-pressure and -temperature experiments in the KMA.

Let us summarize the trends of the present calculation results (Figs. 1 and 2). The electrical resistivity increases linearly with increasing temperature. The linearity continues up to 200 GPa following the Bloch-Grüneisen law, which in turn means that the resistivity saturation is not significant [Fig. 3(a)]. The Seebeck coefficient decreases with temperature and shows the minimum value. The temperature at which the Seebeck coefficient shows the minimum increases with pressure [Fig. 3(b)]. The thermal conductivity increases with temperature at low temperature, and the temperature

dependence becomes small at high temperature [Fig. 3(c)]. The Lorenz number is not a constant, but varies with temperature [Fig. 3(d)]. It increases with temperature and shows the maximum, then decreases. These trends are commonly observed at the pressure and temperature range investigated in this study.

IV. CONCLUSION

We computed the electronic transport properties (electrical resistivity, Seebeck coefficient, and thermal conductivity) of solid face-centered cubic (fcc) Pt by using the KKR-CPA method combined with the alloy analogy [32,33] up to 200 GPa and 4800 K. Ambient pressure results are consistent with the literature data [10–12]. For the convergence with respect to the number of the pseudocomponents, $N_v = 4$ is sufficient to calculate the electrical resistivity and the thermal conductivity, whereas $N_v \geq 12$ is required for the Seebeck coefficient. Our calculations at high pressure are also consistent with the results of previous experiments [24,25]. The electrical resistivity is almost constant along the melting temperature, which is consistent with the previous modeling [25,47]. The Lorenz number exhibits the temperature dependence, and it becomes $L = 3.20 \times 10^{-8} \text{ W } \Omega \text{ K}^{-2}$ at 100 GPa and 2400 K, which is 30% higher than the Sommerfeld value of $L_{\text{Sommerfeld}} \cong 2.445 \times 10^{-8} \text{ W } \Omega \text{ K}^{-2}$. The Seebeck coefficient is insensitive to pressure at the temperature below 1500 K. However, above 1500 K, the Seebeck coefficient exhibits strong pressure dependence. Recent technical developments of multianvil high-pressure experiments can generate over 120 GPa [53] and ~ 4000 K [54]. In such high-pressure and -temperature conditions, special calibration is needed for the temperature measurements using the Pt-Rh thermocouple.

ACKNOWLEDGMENTS

The authors would like to thank Hisazumi Akai for providing the conductivity calculation code implemented in the AKAIKKR package. The authors also thank Sonju Kou for fruitful discussion. This work was supported by JSPS MEXT/KAKENHI Grant No. JP15H05827. We thank two anonymous reviewers for their constructive comments and suggestions.

-
- [1] Y. Fei, A. Ricolleau, M. Frank, K. Mibe, G. Shen, and V. Prakapenka, Toward an internally consistent pressure scale, *Proc. Natl. Acad. Sci. USA* **104**, 9182 (2007).
 - [2] M. Matsui, E. Ito, T. Katsura, D. Yamazaki, T. Yoshino, A. Yokoyama, and K. I. Funakoshi, The temperature-pressure-volume equation of state of platinum, *J. Appl. Phys.* **105**, 013505 (2009).
 - [3] S. Kamada, H. Fukui, A. Yoneda, H. Gomi, F. Maeda, S. Tsutui, H. Uchiyama, N. Hirao, D. Ishikawa, and A. Q. R. Baron, Elastic constants of single crystal Pt measured up to 20 GPa based on inelastic x-ray scattering: Implication for establishment of an equation of state, *C. R. Geosci.* **351**, 236 (2019).
 - [4] M. Murakami, K. Hirose, K. Kawamura, N. Sata, and Y. Ohishi, Post-perovskite phase transition in MgSiO_3 , *Science* **304**, 855 (2004).
 - [5] H. Gomi, K. Ohta, K. Hirose, S. Labrosse, R. Caracas, M. J. Verstraete, and J. W. Hernlund, The high conductivity of iron and thermal evolution of the Earth's core, *Phys. Earth Planet. Inter.* **224**, 88 (2013).
 - [6] T. Inoue, Effect of water on melting phase relations and melt composition in the system Mg_2SiO_4 - MgSiO_3 - H_2O up to 15 GPa, *Phys. Earth Planet. Inter.* **85**, 237 (1994).
 - [7] I. C. Getting and G. C. Kennedy, Effect of pressure on the emf of chromel-alumel and platinum-platinum 10% rhodium thermocouples, *J. Appl. Phys.* **41**, 4552 (1970).

- [8] R. A. Secco, Thermal conductivity and Seebeck coefficient of Fe and Fe-Si alloys: Implications for variable Lorenz number, *Phys. Earth Planet. Inter.* **265**, 23 (2017).
- [9] W. H. Butler and G. M. Stocks, Calculated electrical conductivity and thermopower of silver-palladium alloys, *Phys. Rev. B* **29**, 4217 (1984).
- [10] J. W. Arblaster, Selected electrical resistivity values for the platinum group of metals part I: Palladium and platinum, *Johnson Matthey Technol. Rev.* **59**, 174 (2015).
- [11] N. Cusack and P. Kendall, The absolute scale of thermoelectric power at high temperature, *Proc. Phys. Soc.* **72**, 898 (1958).
- [12] C. Y. Ho, R. W. Powell, and P. E. Liley, Thermal conductivity of the elements, *J. Phys. Chem. Ref. Data* **1**, 279 (1972).
- [13] P. W. Powell, R. P. Tye, and M. J. Woodman, Thermal conductivities and electrical resistivities of the platinum metals, *Platinum Met. Rev.* **6**, 138 (1962).
- [14] M. J. Woodman, The thermal conductivity and electrical resistivity of platinum, *Platinum Met. Rev.* **10**, 132 (1966).
- [15] J. P. Moore and R. S. Graves, Absolute Seebeck coefficient of platinum from 80 to 340 K and the thermal and electrical conductivities of lead from 80 to 400 K, *J. Appl. Phys.* **44**, 1174 (1973).
- [16] A. T. Burkov, A. Heinrich, P. P. Konstantinov, T. Nakama, and K. Yagasaki, Experimental set-up for thermopower and resistivity measurements at 100–1300 K, *Meas. Sci. Technol.* **12**, 264 (2001).
- [17] A. Guan, H. Wang, H. Jin, W. Chu, Y. Guo, and G. Lu, An experimental apparatus for simultaneously measuring Seebeck coefficient and electrical resistivity from 100 K to 600 K, *Rev. Sci. Instrum.* **84**, 043903 (2013).
- [18] J. J. Martin, P. H. Sidles, and G. C. Danielson, Thermal diffusivity of platinum from 300 to 1200 K, *J. Appl. Phys.* **38**, 3075 (1967).
- [19] P. K. Rawat and B. Paul, Simple design for Seebeck measurement of bulk sample by 2-probe method concurrently with electrical resistivity by 4-probe method in the temperature range 300–1000 K, *Measurement* **91**, 613 (2016).
- [20] R. B. Roberts, F. Righini, and R. C. Compton, Absolute scale of thermoelectricity III, *Philos. Mag. B* **52**, 1147 (1985).
- [21] A. A. Rudnitskii, *Thermoelectric Properties of the Noble Metals and Their Alloys* (Izdatelstvo Akademii Nauk SSSR, Moscow, 1956).
- [22] B. Y. Terada, K. Ohkubo, and T. Mohri, Thermal conductivities of platinum alloys at high temperatures, *Platinum Met. Rev.* **49**, 21 (2005).
- [23] M. J. Laubitz and M. V. D. Meer, The thermal conductivity of platinum between 300 and 1000° K, *Can. J. Phys.* **44**, 3173 (1966).
- [24] P. W. Bridgman, The resistance of 72 elements, alloys and compounds to 100,000 kg/cm², *Proc. Am. Acad. Arts Sci.* **81**, 165 (1952).
- [25] R. S. McWilliams, Z. Konôpková, and A. F. Goncharov, A flash heating method for measuring thermal conductivity at high pressure and temperature: Application to Pt, *Phys. Earth Planet. Inter.* **247**, 17 (2015).
- [26] K. Ohta, Y. Kuwayama, K. Hirose, K. Shimizu, and Y. Ohishi, Experimental determination of the electrical resistivity of iron at Earth's core conditions, *Nature* **534**, 95 (2016).
- [27] Z. Konôpková, R. S. McWilliams, N. Gómez-Pérez, and A. F. Goncharov, Direct measurement of thermal conductivity in solid iron at planetary core conditions, *Nature* **534**, 99 (2016).
- [28] D. Dobson, Geophysics: Earth's core problem, *Nature* **534**, 45 (2016).
- [29] X. Sha and R. E. Cohen, First-principles studies of electrical resistivity of iron under pressure, *J. Phys.: Condens. Matter* **23**, 075401 (2011).
- [30] M. Pozzo and D. Alfè, Saturation of electrical resistivity of solid iron at Earth's core conditions, *SpringerPlus* **5**, 256 (2016).
- [31] J. K. Glasbrenner, B. S. Pujari, and K. D. Belashchenko, Deviations from Matthiessen's rule and resistivity saturation effects in Gd and Fe from first principles, *Phys. Rev. B* **89**, 174408 (2014).
- [32] H. Ebert, S. Mankovsky, K. Chadova, S. Polesya, J. Minar, and D. Koedderitzsch, Calculating linear-response functions for finite temperatures on the basis of the alloy analogy model, *Phys. Rev. B* **91**, 165132 (2015).
- [33] S. Kou and H. Akai, First-principles calculation of transition-metal Seebeck coefficients, *Solid State Commun.* **276**, 1 (2018).
- [34] J. Xu, P. Zhang, K. Haule, J. Minar, S. Wimmer, H. Ebert, and R. E. Cohen, Thermal Conductivity and Electrical Resistivity of Solid Iron at Earth's Core Conditions from First Principles, *Phys. Rev. Lett.* **121**, 096601 (2018).
- [35] V. Drchal, J. Kudrnovský, D. Wagenknecht, and I. Turek, Alloy disorder and fluctuating magnetic moments in the Earth's core, *J. Magn. Magn. Mater.* **475**, 767 (2018).
- [36] M. Oshita, S. Yotsuhashi, H. Adachi, and H. Akai, Seebeck coefficient calculated by Kubo-Greenwood formula on the basis of density functional theory, *J. Phys. Soc. Jpn.* **78**, 024708 (2009).
- [37] Y. Wang, Y. J. Hu, B. Bocklund, S. L. Shang, B. C. Zhou, Z. K. Liu, and L. Q. Chen, First-principles thermodynamic theory of Seebeck coefficients, *Phys. Rev. B* **98**, 224101 (2018).
- [38] H. Akai, Fast Korringa-Kohn-Rostoker coherent potential approximation and its application to FCC Ni-Fe systems, *J. Phys.: Condens. Matter* **1**, 8045 (1989).
- [39] J. P. Perdew, K. Burke, and M. Ernzerhof, Generalized Gradient Approximation Made Simple, *Phys. Rev. Lett.* **77**, 3865 (1996).
- [40] W. H. Butler, Theory of electronic transport in random alloys: Korringa-Kohn-Rostoker coherent-potential approximation, *Phys. Rev. B* **31**, 3260 (1985).
- [41] H. Gomi, K. Hirose, H. Akai, and Y. Fei, Electrical resistivity of substitutionally disordered hcp Fe-Si and Fe-Ni alloys: Chemically-induced resistivity saturation in the Earth's core, *Earth Planet. Sci. Lett.* **451**, 51 (2016).
- [42] H. Gomi and T. Yoshino, Impurity resistivity of fcc and hcp Fe-based alloys: Thermal stratification at the top of the core of super-Earths, *Front. Earth Sci.* **6**, 217 (2018).
- [43] A. B. Belonoshko and A. Rosengren, High-pressure melting curve of platinum from *ab initio* Z method, *Phys. Rev. B* **85**, 174104 (2012).
- [44] D. Errandonea, High-pressure melting curves of the transition metals Cu, Ni, Pd, and Pt, *Phys. Rev. B* **87**, 054108 (2013).
- [45] B. Zhang, B. Wang, and Q. Liu, Melting curves of Cu, Pt, Pd and Au under high pressures, *Int. J. Mod. Phys. B* **30**, 1650013 (2016).
- [46] S. Anzellini, V. Monteseuro, E. Bandiello, A. Dewaele, L. Burakovsky, and D. Errandonea, *In situ* characterization of the

- high pressure–high temperature melting curve of platinum, *Sci. Rep.* **9**, 13034 (2019).
- [47] F. D. Stacey and O. L. Anderson, Electrical and thermal conductivities of Fe-Ni-Si alloy under core conditions, *Phys. Earth Planet. Inter.* **124**, 153 (2001).
- [48] O. Gunnarsson, M. Calandra, and J. E. Han, *Colloquium*: Saturation of electrical resistivity, *Rev. Mod. Phys.* **75**, 1085 (2003).
- [49] M. Pozzo and D. Alfè, Electrical resistivity saturation of solid iron at Earth’s core conditions from density functional theory, in *Proceedings of AGU Fall Meeting, San Francisco, CA 2016*, AGU Abstract DI13A-2356 (unpublished).
- [50] Y. Nishihara, K. Fuke, Y. Tange, and Y. Higo, Determination of pressure effect on thermocouple electromotive force using multi-anvil apparatus, *High Pressure Res.* **36**, 121 (2016).
- [51] F. P. Bundy, Effect of pressure on emf of thermocouples, *J. Appl. Phys.* **32**, 483 (1961).
- [52] J. Li, C. Hadidiacos, H. K. Mao, Y. Fei, and R. J. Hemley, Behavior of thermocouples under high pressure in a multi-anvil apparatus, *High Pressure Res.* **23**, 389 (2003).
- [53] D. Yamazaki, E. Ito, T. Yoshino, N. Tsujino, A. Yoneda, H. Gomi, J. Vazhakuttiyakam, M. Sakurai, Y. Zhang, Y. Higo, and Y. Tange, High pressure generation in the Kawai-type multianvil apparatus, *C. R. Geosci.* **351**, 253 (2019).
- [54] L. Xie, A. Yoneda, T. Yoshino, D. Yamazaki, N. Tsujino, Y. Higo, Y. Tange, T. Irifune, T. Shimei, and E. Ito, Synthesis of boron-doped diamond and its application as a heating material in a multi-anvil high-pressure apparatus, *Rev. Sci. Instrum.* **88**, 093904 (2017).